Journal of The Electrochemical Society, **161** (8) E3302-E3310 (2014)
0013-4651/2014/161(8)/E3302/9/$31.00 © The Electrochemical Society

JES Focus Issue on Mathematical Modeling of Electrochemical Systems at Multiple Scales

A Multiscale Model of Electrochemical Double Layers in Energy Conversion and Storage Devices

Matias A. Quiroga,[a,b] Kan-Hao Xue,[a,b] Trong-Khoa Nguyen,[a,b] Michał Tułodziecki,[a,b] He Huang,[a,b] and Alejandro A. Franco[a,b,*,z]

[a]*Laboratoire de Réactivité et Chimie des Solides (LRCS), CNRS UMR 7314, Université de Picardie Jules Verne, 80039 Amiens Cedex, France*
[b]*Réseau sur le Stockage Electrochimique de l'Energie (RS2E), FR CNRS 3459, France*

In this paper we report a statistical-mechanics-based continuum theory allowing tackling the simulation of electrochemical double layers under non-equilibrium conditions at electrolyte/electrode interfaces relevant to electrochemical cells for energy conversion and storage. The present theory is designed to capture the impact onto the overall electrode behavior of the electrolyte composition in terms of solvent, charged polymers and ions concentration, for a large diversity of cases, from diluted solutions to ionic liquids. From its continuum character, the theory is particularly useful for the simulation of interfacial electrochemical mechanisms within multiscale frameworks scaling up atomistic and molecular level properties onto overall performance cell models. Results obtained with our home-made MS LIBER-T simulation package are presented and discussed within the context of fuel cells and lithium ion batteries.

Manuscript submitted March 10, 2014; revised manuscript received April 25, 2014. Published June 4, 2014. *This paper is part of the JES Focus Issue on Mathematical Modeling of Electrochemical Systems at Multiple Scales.*

The charge distribution at the interface between liquid electrolytes and solid electrodes, the so-called electrochemical double layer (EDL), plays a key role in the redox kinetic processes in electrochemical devices for energy conversion and storage. Examples of such devices are fuel cells, rechargeable batteries and super-capacitors. EDLs are formed in a large diversity of forms in these devices, depending on the chemical composition of the electrolyte and the electrode. Electrolytes can have different levels of complexity, as they can be formed by high concentrated ionic solutions (e.g. in lithium ion batteries[1] (LIBs)), moderate concentrated and diluted ionic solutions (e.g. in lithium air batteries[2] (LABs)), mixed media involving ions, solvents and charged polymers (e.g. in polymer electrolyte membrane fuel cells[3] (PEMFCs)) or ions, solvents and additives (e.g. in LIBs),[4] and ionic liquids (e.g. in super-capacitors[5,6] (SCs)). Electrodes can be made of metallic oxide semi-conductors (e.g. in LIBs)[7] or metallic catalysts (e.g. in PEMFCs).[8,9] In these systems, the charge distribution within the EDL is generally time-dependent and affects the effectiveness of the redox reactions (e.g. conversion reactions in batteries) taking place on the electrode, and it is conversely affected by the redox reactions on the electrode and the ionic transport properties of the electrolyte.[10] For instance, it seems unclear how much EDL effects affect the performance of electrochemical devices, as the discharge and charge dynamics of LIBs for example.[11] Furthermore, still in the case of LIBs, understanding these interfacial processes is crucial for tackling the problem of the Solid Electrolyte Interphase (SEI) formation and growing kinetics.[12] Similar questions arise regarding the role of the liquid/solid interfaces onto the electrolyte decomposition kinetics in LABs.[13]

Frumkin and coworkers were the first suggesting that EDL and the effectiveness of the redox reactions affect each other.[14] They have also demonstrated that this strong relationship arises in a complex dependence of the electrode potential on its charge density.[15] Part of literature addresses the question regarding the Frumkin corrections[16–20] additionally accounting for the solvent influence at the interfaces.[14] The modeling and understanding of electrochemical processes taking place at solid electrode/liquid electrolyte interfaces have been struggled for many years. The EDL is typically assumed to exist under equilibrium conditions. For instance, the structure of the EDL is not being affected by the redox reactions, and conversely, the structure of this EDL does not affect the evolution of the redox reactions.

Regarding the modeling of the electrolytes, there is a huge number of works and we avoid here to be exhaustive. In particular, theoretical descriptions at the quantum level are also out of scope of this paper.[21]

The development of continuum theories of EDLs is expected to be useful for the simulation of interfacial electrochemical mechanisms within multiscale frameworks scaling up atomistic and molecular level properties onto overall performance cell models.[22–30] A few attempts have been reported in the literature so far for describing EDLs in fuel cells and in other systems where the ionic transport is usually modeled within the Poisson-Nernst-Planck (PNP) approach under the diluted solution approximation[22,31,32] but without taking into the account the role that solvent may have onto the effective transport properties of the electrolyte.

Numerous continuum theories have been reported since 80 years to describe multi-component liquid mixtures at the bulk level.[33–35] These models have been used and further developed for calculating the static dielectric constant of mixed-solvent electrolyte solutions.[36] There is however a lack of understanding on the structural properties of the liquid mixtures at the vicinity of charged surfaces.

Significant efforts have been already reported for the modeling of ionic distributions at the vicinity of charged surfaces within the context of biological systems.[37,38] Many of these approaches use an equilibrium Poisson-Boltzmann distribution to describe the ionic concentration profiles in polar solvents at the vicinity of charged surfaces. As discussed by Gongadze et al.[37] at the vicinity of the charged surfaces one expects a depletion of the electric permittivity mainly due to the increase of the number of ions, the ion-ion correlation, the finite-size effects and the increase of the solvent dipoles orientation when approaching to the surface. The idea of an inhomogeneous electric permittivity inside the EDL was significantly discussed by Conway, Bockris and others.[39]

Still in the context of biological systems, Abrashkin et al. proposed an approach coarse graining the interaction of individual ions and punctual dipoles.[40] Their so-called Dipolar Poisson-Boltzmann (DPB) approach is able to predict how a single solvent electric permittivity deviates from its bulk value when approaching a charged surface. Although it is done on a mean-field level, their theory includes some aspects of the discrete nature of the dipolar solvent molecules and how they modify the ion–solvent interactions.

Gongadze and Iglic have also proposed a Langevin-Poisson-Boltzmann (LPB) model for point-like ions presenting a water electrolyte solution in contact with a planar charged surface.[41] Their model accounts for the finite size of the involved molecules, the cavity and reaction fields. The authors show that these effects make the

*Electrochemical Society Active Member.
[z]E-mail: alejandro.franco@u-picardie.fr

reduction of permittivity of the electrolyte solution near the charged surface even stronger. Further improvements on their model have been recently proposed.[42] A similar approach has been reported by Levy et al.[43] to study the variation of the dielectric response of a liquid (e.g. water) when a salt is added to the solution at bulk.

Another important aspect that should be considered in EDL simulations is the size of different species. Few models have been proposed within Monte Carlo and mean field approaches[44–48]: however difficulties in mathematical analysis and numerical computation make them unpractical and hard to implement. Killic et al.[49,50] have proposed a model that takes into account the finite size effect based on the PNP theory. In this model species are no more treated as points in the space as the maximum permitted concentration is fixed to $1/a^3$. Although their model includes steric effects, all the species are assumed to have identical size. A similar approach has been followed by Chu et al.[51] who proposed a model based on PB theory for two different sizes of the species. However this PB model has two main drawbacks, for instance i) it is developed only for the systems in equilibrium ii) it becomes mathematically very complex for three and more different sizes of the species. Lu et al.[52] attempted to implement the size effect in a PNP model based on the fluid density functional theory. They arrived to a similar expression as in the Killic et al. model with an additional parameter accounting for the relative size effect (related to the size differences among the species).

Despite significant efforts on developing continuum EDL models mainly in biological systems, there is still a lack of a cohesive theory allowing describing at the continuum level all the known types of EDLs in conditions representative of electrochemical power generators. In this paper we propose such a cohesive theory by introducing a refined treatment of electro-kinetic effects, going beyond the PB and PNP approaches, with particular focus on the solvent non-homogeneous electric field screening at the electrified interface. Derivations of such a model are comprehensively presented and compared to previously developed theories. Furthermore, the application of the model is illustrated for the simulation of an EDL formed at the vicinity of Platinum in a PEMFC cathode, and for the simulation of an EDL formed at the vicinity of a graphite electrode during the de-intercalation process in a LIB. Finally, we conclude and indicate further directions of our work.

Our Theory

Structurally similar to classical EDL models, our EDL model consists of two distinct regions (Figure 1): an external layer (EL) and an inner layer (IL). The EL model describes the ions (here cations) and counter-ions (here anions) transport, affected by the solvent composition and/or the morphology of the charged polymer eventually present in the solution as in the case of PEMFCs. The EL model accounts for both the finite size effect of the species and the relative size effect between them. The IL model describes the coverage evolution of the intermediate reaction species (involved in possible REDOX reactions), adsorbing/desorbing solvent molecules and ions on the electrode surface.

IL model.— The local charge density σ in the electrode in Figure 1 is related to the imposed local electronic current density J through

$$J - J_{FAR} = -\frac{\partial \sigma}{\partial t} \qquad [1]$$

where J_{FAR} is the faradaic current density which is proportional to the algebraic addition of the kinetic rates ν_i associated to electrochemical reactions happening on the surface according to

$$J_{FAR} = F \sum_i (\pm n_i)\, \nu_i \qquad [2]$$

where F is the Faraday constant and n_i is the stoichiometric coefficient. For the kinetic rates we have in general[23]

$$\nu_l = k_l \prod_n a_n^{\alpha_n} - k_{-l} \prod_m a_m^{\alpha_m} \qquad [3]$$

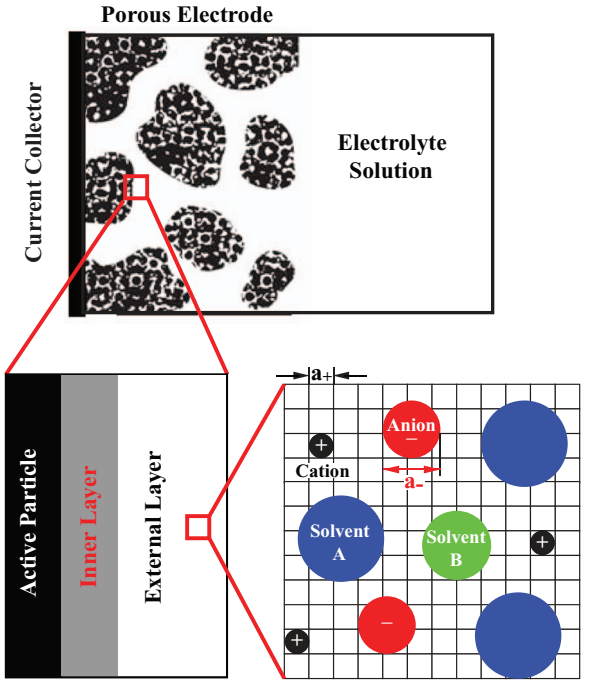

Figure 1. Model implementation scheme with the EDL region.

where a refers to the activity of the reactants (in solution or adsorbed), products (in solution or adsorbed) and intermediate ad-species (coverage), α being the stoichiometry coefficients. In eq. 3 the kinetic parameters k can be given for example by the Eyring's expression from the Transition-State-Theory

$$k_l = \kappa \frac{k_B T}{h} \exp\left(\frac{-E_{act,l} + f(\sigma)}{RT}\right) \qquad [4]$$

where $E_{act,l}$ is the activation energy without influence of the interfacial electric field (it may be estimated from Density Functional Theory -DFT- calculations), κ is the frequency pre-factor (it can include organizational partition functions), k_B and R are the Boltzmann and the ideal gas constants respectively, T is the absolute temperature and h is the Planck constant. f(σ) is a function of the charge density σ, the so-called surface potential different of zero only for electrochemical steps. f(σ) is also proportional to the electrostatic potential drop through the IL between the electrode surface and the electrolyte. We note that the exponential argument, $-E_{act,l} + f(\sigma)$, is an effective activation energy.

By taking into account all the reaction steps, the evolution of the surface concentration of the intermediate reactants and products θ_m is given by the solution of the balance equation

$$K_m \frac{d\theta_m}{dt} = \sum_i n_i \nu_i - \sum_j n_j \nu_j \qquad [5]$$

where K_m is a factor proportional to the maximal number of moles of reaction sites per electrode surface area, given by:

$$K_m = \frac{n^m_{\max}}{N_A} \qquad [6]$$

with

$$n^m_{\max} = \frac{1}{d_m^2} \qquad [7]$$

where d_m^2 is the surface area occupied by the specie m.

The lateral size of an arbitrary specie m is then written as

$$d_m = \sqrt{\gamma_m} d \qquad [8]$$

where γ_m characterizes the occupied surface area ratio of the specie m with respect to the free site on the electrode. In the above equations d^2 refers to the adsorption area of the smallest adspecie.

Note that J_{FAR} impacts the time evolution of σ which affects in turn the kinetic rates in eq. 3. Finally this changes the rate of the elementary steps in eq. 5 affecting J_{FAR}. In order to calculate $f(\sigma)$ for eq. 4 we need to integrate the electric force field across the IL thickness

$$f(\sigma) = \frac{F}{N_A}\int_0^H \vec{E}\cdot d\vec{s} \quad [9]$$

where H refers to the distance between the reaction plane and the electrode surface. Generally speaking, H is related to an electron tunneling probability from the electrode to the reaction plane. The electric field satisfies

$$\vec{E} = \frac{1}{\varepsilon_0}[\vec{D} - \vec{P}] \quad [10]$$

where $\vec{D}$ is the displacement vector and $\vec{P}$ is the dipolar vector. The expression for these vectors in the IL are given by:[53]

$$|\vec{D}| = \sigma_{free} \quad [11]$$

$$\vec{P} = N_A\sum_i \vec{p}_i\cdot c_i \quad [12]$$

where σ_{free} is the surface charge density,$\vec{p}_i$ is the dipolar moment of each type of adsorbed species and c_i is its molar concentration. The total σ_{free} can be written as the addition of the electrode charge density σ and the contribution of adsorbed ions from the electrolyte:

$$\sigma_{free} = \sigma + F\sum_j Z_j c_j \quad [13]$$

where Z_j is the charge value of the ion j. Another important implication from eq. 11 is that the displacement vector only depends on the adsorbed free charge. For simplicity reasons, by assuming that H is constant, and replacing eq. 12 and 13 into eq. 9 and integrating it along a straight path across the IL thickness (by keeping in mind that the path selected do not impact in the result, since the electric field is a conservative field) we arrive to:

$$f(\sigma) = \frac{F}{N_A\varepsilon_0}\left(\sigma + F\sum_j Z_j c_j - \Gamma\right)H \quad [14]$$

where Γ is the dipolar contribution to the total electrostatic potential jump through the IL. Γ is a function of the coverage of intermediate reaction species and of solvent adsorbed molecules. The contribution to Γ coming from the coverage of the intermediate reaction species θ_m is given by the solution of eq. 5.

If we neglect the first one, we can write

$$\Gamma = \frac{1}{H}\sum_i p_i(\overrightarrow{\theta}_i - \overleftarrow{\theta}_i) \quad [15]$$

where $\overrightarrow{\theta}_i$ and $\overleftarrow{\theta}_i$ refer to the coverage of solvent molecules pointing to the electrode surface and to the electrolyte respectively. In the case we have solvents with different sizes, their coverage can be defined as

$$\overrightarrow{\theta}_i = \frac{\gamma_i\overrightarrow{n}_i}{n_{\max}} \quad [16]$$

and

$$\overleftarrow{\theta}_i = \frac{\gamma_i\overleftarrow{n}_i}{n_{\max}} \quad [17]$$

The coefficient γ_i indicates the number of free sites that a species i will occupy when it is adsorbed, closely related to the size of i (see Figure 1) and where $n_{max} = 1/d^2$. For simplicity we only assume two possible directions for the solvent dipoles both perpendicular to the electrode surface: the dipole moment pointing toward the surface or opposite to the surface. The free site coverage is defined similarly as

$$\theta_s = \frac{n_s}{n_{\max}} \quad [18]$$

therefore the normalization condition is

$$\theta_s + \sum_i(\vec{\theta}_i + \overleftarrow{\theta}_i) + \sum_m \theta_m = 1 \quad [19]$$

where θ_m is the surface coverage of, if exists, an intermediate reaction product m.

In order to calculate the surface coverage of the solvent, we consider the following surface adsorption equilibrium reactions

$$solvent_i + \gamma_i s \leftrightarrow \overrightarrow{solvent_i - s} \quad [20]$$

with activation energy $\Delta\vec{G}_i$ and the inversed adsorption reaction

$$solvent_i + \gamma_i s \leftrightarrow \overleftarrow{solvent_i - s} \quad [21]$$

with activation energy $\Delta\overleftarrow{G}_i$. By considering as an example the adsorption reaction in [20] the law of mass action requires

$$\frac{\vec{n}_i}{n_{\max}} = a_i\left(\frac{n_s}{n_{\max}}\right)^{\gamma_i}\exp\left(-\frac{\Delta\vec{G}_i}{RT}\right) \quad [22]$$

where a_i is the dimensionless "activity" of solvent i in the solution. Combining [16], [18], and [22] yields

$$\vec{\theta}_i = \gamma_i a_i\theta_s^{\gamma_i}\exp\left(-\frac{\Delta\vec{G}_i}{RT}\right) \quad [23]$$

For the other adsorption direction it follows similarly

$$\overleftarrow{\theta}_i = \gamma_i a_i\theta_s^{\gamma_i}\exp\left(-\frac{\Delta\overleftarrow{G}_i}{RT}\right) \quad [24]$$

Following the previous work of Franco et al.,[22] the activation energy can be expressed in three distinct terms:

$$\Delta\vec{G}_i = \Delta\vec{G}_i^{chem} + \Delta\vec{G}_i^{elect} + \Delta\vec{G}_i^{inter} \quad [25]$$

where the chemical term ΔG_i^{chem} is independent of the adsorption direction

$$\Delta\vec{G}_i^{chem} = \Delta\overleftarrow{G}_i^{chem} = \Delta G_i^{chem} \quad [26]$$

In the case that the adsorbed species are all solvent molecules which are dipoles but as a whole electroneutral, both the dipole-surface electrical term ΔG_i^{elect} and the species-interaction term are odd functions of the adsorption direction:

$$\Delta\vec{G}_i^{elect} = -\Delta\overleftarrow{G}_i^{elect} \quad [27]$$

$$\Delta\vec{G}_i^{inter} = -\Delta\overleftarrow{G}_i^{inter} \quad [28]$$

Hence, the latter two terms can be collected together to simplify the notation. In this work we neglect the adsorption of charged species on the surface. Define X_i to be

$$X_i = \frac{\Delta\vec{G}_i^{elect} + \Delta\vec{G}_i^{inter}}{RT} \quad [29]$$

then the difference between the two surface coverage with opposite directions is

$$\vec{\theta}_i - \overleftarrow{\theta}_i = 2\gamma_i a_i\theta_s^{\gamma_i}\exp\left(-\frac{\Delta G_i^{chem}}{RT}\right)\sinh(-X_i) \quad [30]$$

Nevertheless, the value X_i remains to be solved. For the dipole-surface part, since the electrostatic energy between a dipole $\overrightarrow{p}$ in an applied electric field $\overrightarrow{E}$ is $-\overrightarrow{p}\cdot\overrightarrow{E}$, in an one-dimensional problem

ΔG_i^{elect} is simply written as

$$\Delta \overrightarrow{G}_i^{elect} = \frac{N_A p_i \sigma}{\varepsilon_0} \quad [31]$$

$$\Delta \overleftarrow{G}_i^{elect} = -\frac{N_A p_i \sigma}{\varepsilon_0} \quad [32]$$

For the dipole-dipole interaction part, we extend the previous work of Franco et al.[31] from a single solvent case (water) to the multiple solvent case, and by assuming the eventual surface intermediate reaction species with a dipolar moment negligible compared to the ones of the solvents[c]

$$\Delta \vec{G}_i^{inter} = N_A \sum_j W_{i\to j}(\vec{\theta}_j - \overleftarrow{\theta}_j) \quad [33]$$

where $W_{i\to j}$ is the energy needed to insert a *i* solvent molecule oriented to the surface into an adlayer of fully covered with *j* dipoles oriented in the same direction that the adsorbing dipole. In practice the pre-adsorbed *j* dipoles may also be oriented in the opposite direction, thus both directions are considered, weighted by the corresponding surface coverage. A further extension of Franco et al.[31] theory leads to the expression of $W_{i\to j}$ as

$$W_{i\to j} = \frac{\nu_j^{-\frac{3}{2}} p_i p_j}{2\pi \overline{\varepsilon_{EL}} d^3} \zeta(3) \quad [34]$$

where ζ is Riemann Zeta-function and where $\overline{\varepsilon_{EL}}$ is the spatial average of the external layer electric permittivity. The parameter $\gamma_j^{-\frac{3}{2}}$ is responsible for the different sizes of various species.

Finally, we combine [29]-[34] to obtain the coupled transcendental equation for X_i

$$X_i = \frac{p_i \sigma}{\varepsilon_0 kT} + \frac{p_i \varsigma(3)}{2\pi \overline{\varepsilon_{EL}} kT d^3} \times \sum_j \left[a_j \gamma_j^{-1/2} p_j \theta_s^{\gamma_j} \exp\left(-\frac{\Delta G_j^{chem}}{RT}\right) \sinh(-X_j) \right] \quad [35]$$

where the summation runs over all other solvent species *j* different from *i*. Regarding the unknown variable θ_s, eqs. 19 and 30 lead to,

$$\theta_s = 1 - \sum_i (\vec{\theta}_i + \overleftarrow{\theta}_i) - \sum_m \theta_m = 1 - 2\sum_i \left[\gamma_i a_i \theta_s^{\gamma_i} \exp\left(-\frac{\Delta G_i^{chem}}{RT}\right) \cosh(-X_i) \right] - \sum_m \theta_m \quad [36]$$

After calculating X_i, Γ is obtained from equation 15

$$\Gamma = \frac{2}{d^2 H} \sum_i \gamma_i a_i p_i \theta_s^{\gamma_i} \exp\left(-\frac{\Delta G_i^{chem}}{RT}\right) \sinh(-X_i) \quad [37]$$

EL model.— The equations describing the charge distribution in the EL are derived from the minimization of the free energy functional $F = U - TS$ written in terms of the electrostatic potential and the mobile particles concentration in the electrolyte (ions, solvents, polymers). The entropic term (*TS*) relates to the total number of spatial configurations that the mobile particles can adopt over the available sites

$$TS = k_B T \ln(W) \quad [38]$$

where *W* is the number of combinations for the distribution of *i* types of particles in a regular grid (cf. Figure 1). Let us consider a species N_1 with an effective size β_1 that fill in the grid with free slots of constant size. We assume that the β_1 is an integer number and describes the amount of slots that the species take. The number of possibilities to fill the grid by the N_1 species can be written as:

$$\begin{aligned} &N_t (N_t - \beta_1)(N_t - 2\beta_1) \ldots (N_t - (N_1 - 1)\beta_1) \\ &= \beta_1^{N_1} \frac{N_t}{\beta_1} \left(\frac{N_t}{\beta_1} - 1\right) \left(\frac{N_t}{\beta_1} - 2\right) \ldots \left(\frac{N_t}{\beta_1} - N_1 + 1\right) \\ &= \frac{\beta_1^{N_1} \left(\frac{N_t}{\beta_1}\right)!}{N_1! \left(\frac{N_t}{\beta_1} - N_1\right)!} \end{aligned} \quad [39]$$

By defining *n* as the total amount of different species a general formula can be written:

$$W = \prod_i^n \frac{\beta_i^{N_i} \alpha_i!}{N_i! \delta_i!} \quad [40]$$

where

$$\alpha_i = \frac{N_t}{\beta_i} - \sum_{\substack{j=1 \\ i\geq 2}}^{i-1} \left(\frac{\beta_j N_j}{\beta_i}\right) \quad [41]$$

$$\delta_i = \frac{N_t}{\beta_i} - \sum_{\substack{j=1 \\ i\geq 2}}^{i-1} \left(\frac{\beta_j N_j}{\beta_i}\right) - N_i \quad [42]$$

where N_t is the total number of meshes accounted in the grid and β_j is the relative size between each particle and the mesh size. Therefore the N_t can be expressed as:

$$N_t = \sum_i \beta_i N_i + N_h \quad [43]$$

where N_h is the number of holes.

In order to express the entropy in terms of the concentration of each type of particle, we define $N_t = Va^{-3}$ and $N_i = N_A c_i N_t a^3$ where V is the total volume of the EL, c_i is the concentration for the *i* type of particle. By using the Stirling's formula ($ln(M!) \approx M\, ln(M) - M$) and replacing $V \to dV$ to describe the local contribution to the total entropy, we have

$$\begin{aligned} -TS = \frac{RT}{N_A} \int dV \Bigg[&\sum_{i=1}^n c_i \ln(c_i a^3 N_A) + \frac{1}{a^3 \beta_n} \left(1 - \sum_{j=1}^n \beta_j c_j a^3 N_A\right) \\ &\times \ln\left(1 - \sum_{j=1}^n \beta_j c_j a^3 N_A\right) - \frac{1}{a^3} \sum_{\substack{k=1 \\ i\geq 2}}^{n-1} \left(\frac{\beta_k - \beta_{k+1}}{\beta_k \beta_{k+1}} \right. \\ &\left. \times \left(1 - \sum_{l=1}^k \beta_l c_l a^3 N_A\right) \ln\left(1 - \sum_{l=1}^k \beta_l c_l a^3 N_A\right)\right)\Bigg] \end{aligned} \quad [44]$$

Now we are able to calculate the entropy contribution to the chemical potential following a similar methodology as in,[54] thus:

$$\mu_i = \frac{\partial F}{\partial c_i} = \frac{\partial U}{\partial c_i} + RT \left[ln(c_i a^3 N_A) - \frac{\beta_i}{\beta_n} \ln\left(1 - \sum_{j=1}^n \beta_j c_j a^3 N_A\right) + \sum_{k=i}^{n-1} \left[\frac{\beta_k - \beta_{k+1}}{\beta_k \beta_{k+1}} \beta_i \ln\left(1 - \sum_{l=1}^k \beta_l c_l a^3 N_A\right)\right]\right] \quad [45]$$

Note that if we set all $\beta = 1$ by considering only one type of ion and one type of counter-ion both with identical size, we recover the same expression as derived in.[54–56]

The internal energy (*U*) can be written in general

$$U = \sum_{ij} a_{lj} c_l c_j + F \sum_i z_i c_i \varphi - N_A \sum_i c_i \vec{p}_i \cdot \vec{\nabla} \varphi \quad [46]$$

[c]This assumption is not restrictive and is made here for the sake of simplicity. In order to consider the contribution of the dipolar moment of the intermediate reaction species, a Monte Carlo-like approach should be adopted (this will be discussed by us in an incoming publication).

where a_{ij} is the interaction energy between particles of type i and j, φ is the electrostatic potential and $\vec{p}_i$ is the effective dipolar moment of the particle of type i in the EL.

Now within the framework of the first order non-equilibrium thermodynamics, we can postulate that the molar flux of particles of type i is given by

$$\vec{J}_i = -\frac{D_i}{RT} c_i \vec{\nabla}\mu \qquad [47]$$

where D_i is the diffusion coefficient. The corresponding balance equation provides the solution of c_i

$$\frac{\partial c_i}{\partial t} = -\vec{\nabla}\cdot\vec{J}_i + S_i \qquad [48]$$

where S_i refers to a sink term related to eventual homogeneous chemical reactions in the EL (e.g. electrolyte decomposition reactions in LIBs), which is zero if the electrolyte is chemically stable.

By writing ${}^{D_i}/_{RT} = B_i$ and by combining eqs. 45, 46, 47, and 48, we derive a generalized NP equation governing the species transport,

$$\begin{aligned}\frac{\partial c_i}{\partial t} &= B_i RT\nabla^2 c_i + B_i\vec{\nabla}\cdot\left(c_i\vec{\nabla}\sum_i a_{ij}c_j\right) + B_i z_i F\vec{\nabla}\cdot(c_i\vec{\nabla}\varphi)\\ &\quad -N_A B_i\vec{\nabla}\cdot(c_i\vec{\nabla}(\vec{p}_i\cdot\vec{\nabla}\varphi))\\ &\quad +f_1(\beta_i, c_i) - f_2(\beta_i, c_i)\end{aligned} \qquad [49]$$

In the above expression f_1 and f_2 are given by

$$f_1(\beta_i, c_i) = B_i RT\frac{\beta_i}{\beta_n}\vec{\nabla}\cdot\left(\frac{c_i}{1-\sum_{j=1}^{n} N_a\beta_j c_j a^3}\sum_{j=1}^{n} N_a\beta_j\vec{\nabla}c_j a^3\right) \qquad [50]$$

$$f_2(\beta_i, c_i) = B_i RT\sum_{k=i}^{n-1}\left(\frac{\beta_k-\beta_{k+1}}{\beta_k\beta_{k+1}}\beta_i\vec{\nabla}\cdot\left(\frac{c_i}{1-\sum_{l=1}^{k} N_a\beta_l c_l a^3}\sum_{l=1}^{k} N_a\beta_l\vec{\nabla}c_l a^3\right)\right) \qquad [51]$$

The terms on the right side of eq. 49 represent: the first one is the contribution from the configurational entropy term and is already present in the classical NP equation; the second one accounts for the interaction energy among the species and is one of the extensions of the NP approach provided by the present work; the third one represents the electro-migration; meanwhile, the fourth one accounts for the dipoles interaction with the electric field and represents another extension of the NP approach arising from our work. The last two terms f_1 and f_2 account for the finite and relative size effects. By taking the particular case of $\beta = 1$, the f_2 term becomes zero and we recover the same ion transport expression derived in.[50,57,58] Note that in our case the relative size effect is included in an additional term unlike to Lu and Zhou's model,[46] where this effect appears in the term of finite size effect.

In order to separate the contribution of the ions and the polar solvent in the charge term of the Poisson equation, we split it into free charge (displacement) and polarization charge

$$\varepsilon_0\vec{\nabla}.\vec{E} = -\varepsilon_0\nabla^2\varphi = F\sum_i z_i c_i - N_A\sum_s[(\vec{\nabla}.\vec{p}_s)c_s + \vec{p}_s.\vec{\nabla}c_s] \qquad [52]$$

We underline that, in contrast to the classical Poisson equation, eq. 52 is independent on the average electric permittivity of the electrolyte $\varepsilon = \varepsilon_r\varepsilon_0$. Note that here $\vec{p}_s$ refers to the effective orientational dipolar moment of the solvent molecule s or, in the case of ionic liquids, the dipolar moment of the ion.[59] The orientational dipolar moment is a function of the electric field $-\vec{\nabla}\varphi$. Part of the literature has also treated the non-constant electric permittivity,[60,61] however, the last term in eq. 52 is not accounted. We are convinced in its significance, especially at high electric field, where most of the dipoles are well oriented with the electric field, and the only contribution from the dipolar vector comes from the decoupled charge due to the solvent concentration gradient. Now, for simplicity if we assume that the solvent concentration is constant, we have

$$\vec{\nabla}.\left(-\varepsilon_0\vec{\nabla}\varphi + N_A\sum_s\vec{p}_s c_s\right) = F\sum_i z_i c_i \qquad [53]$$

By knowing that

$$\vec{D} = -\varepsilon_0\vec{\nabla}\varphi + N_A\sum_s|\vec{p}_s|\left(\frac{-\vec{\nabla}\varphi}{|\vec{\nabla}\varphi|}\right)c_s = -\varepsilon\vec{\nabla}\varphi \qquad [54]$$

we get

$$\varepsilon = \varepsilon_0 + N_A\sum_s\frac{|\vec{p}_s|}{|\nabla\varphi|}c_s \qquad [55]$$

which translates the fact that the electric permittivity is not homogenous within the EL. The effective solvent orientational dipolar moment in the direction of the electric field is assumed to follow a Langevin-Boltzmann statistics:[62]

$$\vec{p}_s = -p_s^o\Im\left(\frac{p_s^o|\vec{\nabla}\varphi|}{k_B T}\right)\frac{\vec{\nabla}\varphi}{|\vec{\nabla}\varphi|} \qquad [56]$$

where $\Im$ is the Langevin function ($\Im(Y) = \coth(Y) - 1/Y$) and p_{si}^o is the magnitude of the dipole i.

The corresponding electric permittivity profile in terms of the electric field for different solvents composition is presented in Figure 2. We notice that the electric permittivity significantly deviates from its bulk value with the electric field magnitude.

In Table III we summarize the mean characteristics of our theory in comparison to the classical PNP approach and previously reported extended PNP approaches in the literature.[50,57]

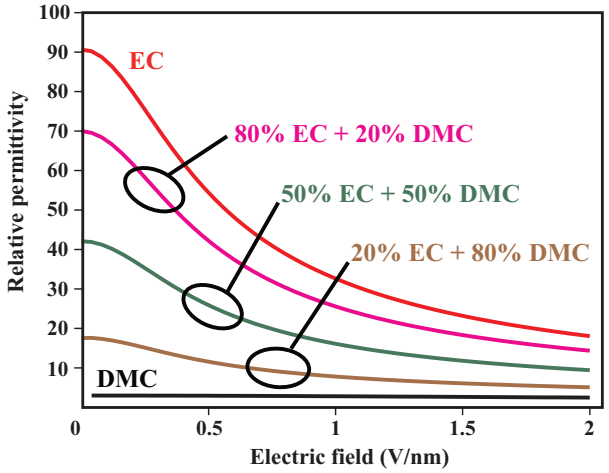

Figure 2. Electric permittivity calculated as function of the electric field for different solvent compositions.

Illustrative Results

We consider here one-dimensional steady-state systems with an EDL thickness between 5 Å and 25 Å. The number of involved particles is in the range of Avogadro's number. As it has been done for similar system in the literature,[63] the selected systems justified the implementation of a continuum model, since, the atomistic models are not able to be implanted in this range. The simulation has been

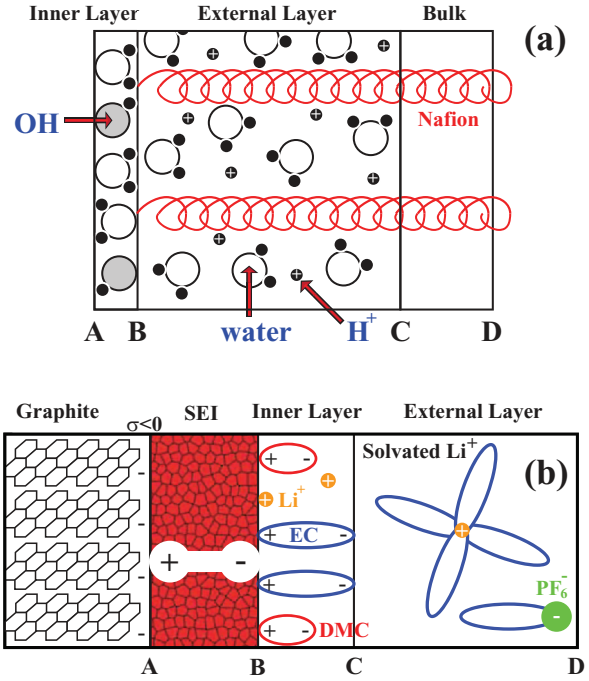

Figure 3. Representative scheme for the simulated electrode/electrolyte interfaces in (a) a PEMFC and (b) in a LIB.

carried out by Matlab modules integrated in the in-house MS LIBER-T simulation package (www.modeling-electrochemistry.com). In the following, we present the application of our theory for two particular cases illustrated schematically in Figure 3:

- simulation of an EDL in a PEMFC cathode during an oxygen reduction reaction (ORR), with water in both IL and EL and where we solve the transport of a single ion (proton);
- simulation of an EDL in a LIB negative electrode during discharge, assuming an intercalation material with negligible volume expansion and considering the mixture of two different solvents. In this case we solve the transport of lithium ion and counter-ion.

For the two cases, results are compared with the ones obtained by the classical PNP theory under the diluted solution approximation. We would like to note that, although we gave the expression for the size effect in EL, we do not include it in the simulations below. Its inclusion will be presented in our next paper on EDL in ionic liquid media.

Theory applied to the PEMFC case.— In the IL we assumed two reactions steps for the ORR as following: $O_2 + 2H^+ + 2e^- + 2s \rightarrow 2OH_{ads}$ and $OH_{ads} + H^+ + e^- \rightarrow H_2O + s$. Along the EDL only water was considered to have an effective dipolar moment. The coverage of the different species involved in the IL was obtained by adding eq. 3 into eq. 5 and considering them to be in the steady state. The kinetic rates were obtained by combining eqs. 4, 11, and 37. Meanwhile, in the EL the description of the proton transport was given by eqs. 49 and 52 in one dimension. The water concentration profile was assumed to be constant all along the EL.

More details about the multiscale simulation methodology can be found in Ref. 23 and 64. All the parameters values used are reported in Table I.

Theory applied to the LIB case.— For the LIB simulations we have considered the following de-intercalation reaction $Li - \Theta^+ \rightarrow Li^+ + \Theta$. Simulations have been carried out for electrolytes with different solvent compositions: EC, EMC and DMC. The coverage for

Table I. List of parameters implemented for the polymer electrolyte fuel cell.

Parameter	Description	Value used
p_{H_2O}	Dipolar moment of water	5.6×10^{-30} C · m
β_+	Proton size effect coefficient	1
C_{H_2O}	Concentration of water	55000 mol · m^{-3}
d	Water molecule size	1×10^{-9} m
E_1	Activation energy first step of the ORR mechanism	80000 J · mol^{-1}
E_2	Activation energy second step of the ORR mechanism	79500 J · mol^{-1}
L	External layer thickness	25×10^{-10} m
H	Inner layer thickness	2×10^{-10} m
T	Temperature	350 K
ε_{DL}	Average electric permittivity for diffuse layer in the classical PNP	80 ε_O
D	Proton diffusion coefficient	1×10^{-9} $m^2 \cdot s^{-1}$

the different solvents is calculated from eq. 23 and eq. 24. Ions and counter-ions transports are calculated from eq. 49 and eq. 52. Solvents composition was assumed to be homogeneous.

All the parameters values are reported in Table II. In particular, E_F^0 is the energy required for an Li ion to get rid of its solvation sphere, which dominates the activation energy of the intercalation reaction. On the other hand, E_B is the activation energy for the de-intercalation reaction.

Numerical results.— In Figure 4a, we report the calculated steady-state proton concentration profiles across the EL in the PEMFC case, using the classical PNP approach and the theory reported in this paper. For both theories we fixed the proton concentration at x = −25 Å to 1200 mol · m^{-3}. We note that with our model we obtain in the EL a lower net charge in comparison to the PNP approach, which can be explained on the basis of the Poisson equation. For instance, as shown in Figure 5a, our theory predicts a lower permittivity near the IL: then less net charge is required to maintain the electric field gradient in the EL.

Table II. List of parameters implemented for the Lithium ion battery.*[65]

Parameter	Description	Value used
E_F^0	Activation energy for intercalation reaction	4000 J · mol^{-1}
E_B	Activation energy for de-intercalation reaction	1000 J · mol^{-1}
d	Solvent molecule size	4×10^{-10} m
p_{EC}	Dipolar moment of EC	3.12×10^{-29} C · m*
p_{DMC}	Dipolar moment of DMC	5.06×10^{-30} C · m*
p_{EMC}	Dipolar moment of EMC	6.92×10^{-30} C · m*
V_{EC}	EC relative size	1
V_{DMC}	DMC relative size	1
V_{EMC}	EMC relative size	1
a_{EC}	EC activity	0.5
a_{DMC}	DMC activity	0.5
a_{EMC}	EMC activity	0.5
D_+	Li^+ diffusion coefficient in electrolyte	1×10^{-10} m^2/s
D_-	Anion diffusion coefficient in electrolyte	1×10^{-9} m^2/s
ΔG_{EC}^{chem}	Adsorption energy for EC	20000 J · mol^{-1}
ΔG_{DMC}^{chem}	Adsorption energy for DMC	25000 J · mol^{-1}
ΔG_{EMC}^{chem}	Adsorption energy for EMC	20000 J · mol^{-1}
L	External layer thickness	5×10^{-10} m
H	Inner layer thickness	5×10^{-10} m
H_{SEI}	SEI thickness	5×10^{-10} m
T	Temperature	298 K

Table III. Summary of the assumption done in different EDL models.

PNP	Previously reported modified PNP[50,57]	Our Model
Non-equilibrium	Non-equilibrium	Non-equilibrium
Punctual ions	One type of finite size ions	Multiple size species
Constant electric permittivity	Constant electric permittivity	Non-constant electric permittivity
Non-interaction energy among different species	Non-interaction energy among different species	Interaction energy among the species
Single type of electrostatic particles: ions	Single type of electrostatic particles: ions	Multiple types of electrostatic particles: ions, dipoles, charged dipoles

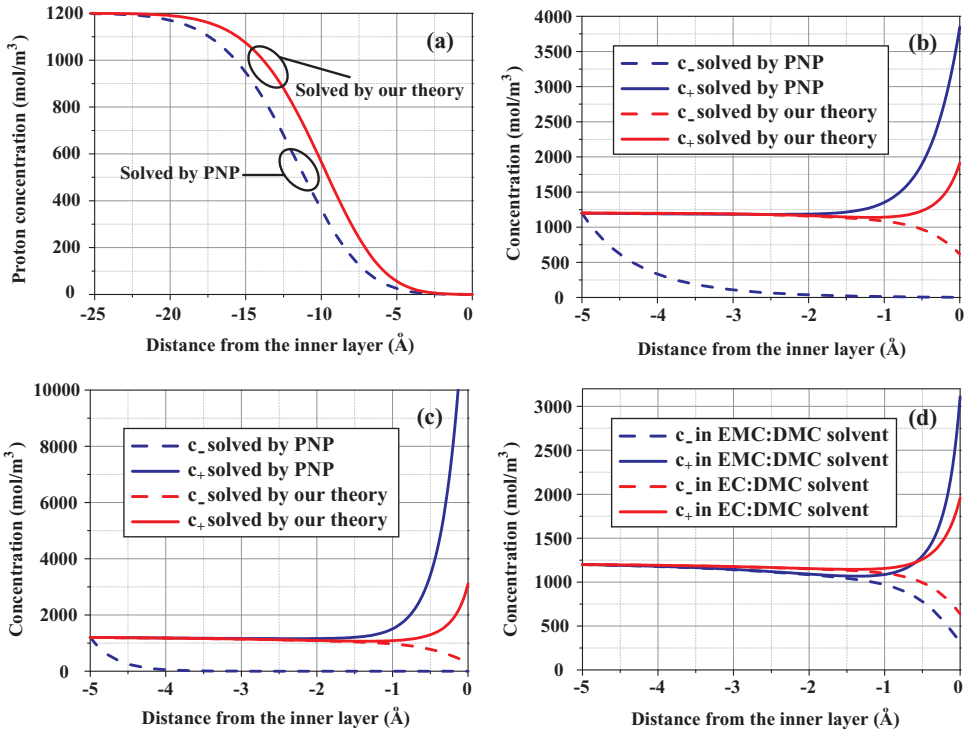

Figure 4. (a) Simulated steady-state proton concentration profiles across the external layer of the fuel cell model, using either PNP or our theory. The surface charge density on the electrode is $\sigma = 0.005$ C/m^2. (b) Simulated steady-state ion concentration profiles across the external layer of the intercalation electrode in the battery model, using either PNP or our theory. The solvent is EC:DMC in mass ratio 4:1. (c) Simulated steady-state ion concentration profiles across the external layer of the intercalation electrode in the battery model, using either PNP or our theory. The solvent is EMC:DMC in mass ratio 4:1 and the electrode surface charge density is $\sigma = -0.008$ C/m^2. (d) Simulated steady-state ion concentration profiles across the external layer of the intercalation electrode in the battery model, using our theory. The solvent is either EC:DMC or EMC:DMC both in mass ratio 4:1 and the electrode surface charge density is $\sigma = -0.008$ C/m^2.

For the LIB case, regardless of the solvent used, Figures 4b and 4c show drastic differences in outer layer simulation results between PNP and our theory. First, PNP gives much higher Li^+ concentration near the IL than our theory, while for anions the opposite trend is discovered. This can be explained by the over-estimated electrolyte permittivity near the IL for the PNP approach, where a constant solvent permittivity is used, regardless of the external electric field. In our theory, however, close to the IL a strong electric field is present, which lowers the electrolyte permittivity significantly. To maintain the same steady-state, our theory requires much less net charge (c_+ - c_-) close to the IL. Secondly, the anion concentration in our theory is smoothly varying from the bulk value, near the bulk solution, to a lower

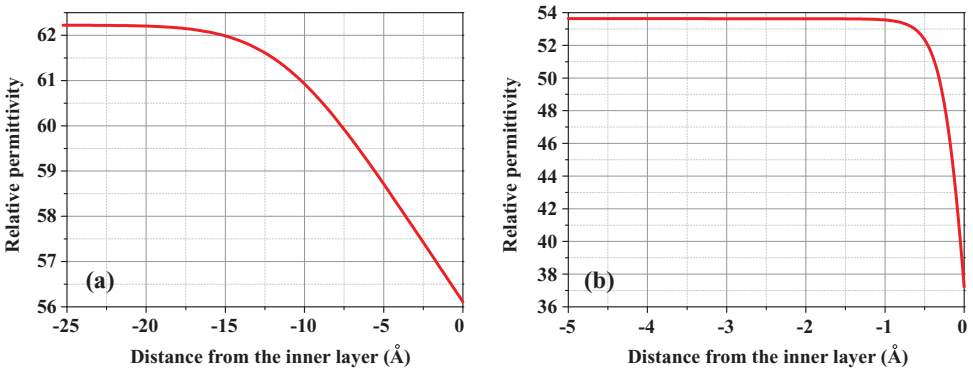

Figure 5. Spatial variation of relative permittivity across the steady-state external layer calculated by our theory for: (a) the fuel cell model at $\sigma = 0.005$ C/m^2; (b) the battery model with EC:DMC mass ratio of 4:1 at $\sigma = -0.008$ C/m^2.

value, near the IL. Yet, PNP gives a discontinuous spatial derivative of anion concentration at the junction between the EL and the bulk solution, which seems artificial due to the choice of diffuse layer thickness as well as the boundary condition. Hence, our theory has better adaptability to the boundary condition of constant salt concentration in the bulk solution. Fig. 4d shows that within the same approach, i.e., our theory, the net charge near the IL will increase if there is an absence of highly polar solvents in the electrolyte solution. Indeed, while EMC and DMC both possess small dipole moments, the inclusion of EC may greatly reduce the maximum lithium concentration in the EDL, therefore lowering the risk of salt precipitation. This phenomenon can be attributed to the increasing of the electric field for the EMC:DMC case, close to the IL which produce a higher net charge in this region.

In Figure 5b, we report the spatial variation of relative permittivity across the steady-state EL calculated by our theory for the LIB case. The calculated permittivity monotonically decreases from its bulk value when approaching to the electrode surface. The deviation magnitude from the bulk value generally depends on the charge density applied to the electrode, the electrolyte solvent composition, etc. making our model more relevant in the field of electrochemical power devices with high electrode/electrolyte interfacial complexity.

Conclusions

In the present paper we have proposed a general EDL theory which applies to a large diversity of types of electrolytes used in electrochemical power generators, such as batteries, fuel cells and supercapacitors. The theory describes how interfacial electrolyte/electrode redox reactions impact the EDL structure (charge distribution) and conversely, how the EDL structure affects the effectiveness of the interfacial redox reactions. In the case of PEMFC, the EDL complexity is due to the concentration of sulfonic acid groups involved that one can have,[3] plus all the intermediate species in the ORR. In the case of LIB, the EDL may have different types of solvents, with different sizes of solvation spheres. The comparison between the theory in this paper and the ones previously reported can be summarized as follows:

(-) classical description of the EDL neglects size effects of different adsorbed species and introduces semi-empirical assumptions in considering the electric permittivity. Our theory accounts for the size effects and relative size effects in both the IL and EL and calculates explicitly the impact of its electrostatic properties onto the effective interfacial reaction kinetics;

(-) classical PNP approaches consider electric permittivity as constant along the EL. Our theory explicitly calculates the electric permittivity along the EDL as function of the electrolyte composition and the local value of the electric field. Cases of no uniform solvent composition can be additionally considered (not shown in this paper). Moreover, our theory recovers the classical PNP equations in the range of diluted solutions at low electric field.

The addition of interaction energy terms into the description of the total internal energy of the electrolyte allow us to considering applying the present model to a wide range of high concentrated electrolytes such as ionic liquids.

In the future further studies will be done by considering the impact of the salt concentration onto the electric permittivity, and by considering of other dipolar orientation statistics (further than Langevin's one). Further works by us consisting of applying our EDL theory for the multiscale simulation of batteries and fuel cells are in progress.[66,67]

Acknowledgments

The authors deeply acknowledge the funding by the 7th Framework Programme of the European Commission in the context of the Fuel Cells and Hydrogen Joint Undertaking (FCH JU) through the project PUMA-MIND FP7 303419, by the ANR Project ALIBABA (reference ANR-11-PRGE-0002) and by the European Research Institute ALISTORE. The authors gratefully acknowledge Prof. J.-M. Tarascon (Collège de France, Paris, France), Prof. D. Larcher, Dr. Abdel El Kharbachi (LRCS, Amiens, France) and Dr. M.-L. Doublet (ICG, Montpellier, France) for helpful discussions. Prof. J.-P. Chehab and Dr. Y. Mammeri (LAMFA, Amiens, France) are also acknowledged for helpful discussions regarding numerical algorithms.

List of Symbols

Symbol	Parameter name	Unit	Value used
J	Current density	$A \cdot m^{-2}$	
J_{FAR}	Faradaic current density	$A \cdot m^{-2}$	
σ	Electrode surface charge density	C · m-2	
F	Faraday constant	$C \cdot mol^{-1}$	96485
v_i	electrochemical reaction rates	$m^{-2} \cdot s^{-1}$	
a_i	Activity coefficient of specie i	m^{-3}	
α	Stoichiometry coefficient		
h	Planck constant	$J \cdot s$	6.62×10^{-34}
k	Kinetic parameter	$mol^{0.5} \cdot m^{-0.5} \cdot s^{-1}$	
N_A	Avogadro's number	mol^{-1}	6.02×10^{23}
κ	Frequency factor		
$E_{act,l}$	activation energy	$J \cdot mol^{-1}$	
$f(\sigma)$	Electrostatic surface potential	V	
H	Reaction plane distance from the electrode	m	
K_m	Maximal number of moles of reaction sites per unit surface area	$mol \cdot m^{-2}$	
$\vec{E}$	Electric field vector	$V \cdot m^{-1}$	
$\vec{D}$	Displacement field vector	$C \cdot m^{-2}$	
$\vec{P}$	Polarization field vector	$C \cdot m^{-2}$	
z_j	Charge value		
c_i	Concentration of i specie	$mol \cdot m^{-3}$	
ε_0	Vacuum permittivity	$F \cdot m^{-1}$	8.854×10^{-12}
Γ	Dipolar term into the electrostatic surface potential	$C \cdot m^{-2}$	
d	Effective lateral size of adsorbed specie		
ν_i	Surface area ratio		
$\vec{\theta}_i$, $\overleftarrow{\theta}_i$	Surface coverage of adsorbed solvent according to their dipole orientation		
$\Delta\vec{G}_i$, $\Delta\overleftarrow{G}_i$	Activation energy according to the dipolar orientation	$J \cdot mol^{-1}$	
X_l	variable of the transcendental equation [31]		
R	Universal gas constant	$J \cdot mol^{-1}\ K^{-1}$	8.31
ς	Riemann Zeta-function		
k_B	Boltzmann constant		R/N_A
W	Combination number for the distribution of the particles		
a^3	Volume of the smallest specie in the EL		
β_i	Effective size of the i specie		1
α_i	Finite size term into W		
δ_i	Relative size term into W		
φ	Electrostatic potential	V	

D_i	Diffusion coefficient	$m^2 \cdot s^{-1}$
f_1	Finite size term in our theory	
f_2	Relative size term in our theory	
$\Im$	Langevin function	

References

1. J. M. Tarascon and D. Guyomard, *Solid State Ion.*, **69**, 293 (1994).
2. Z. Peng, S. A. Freunberger, Y. Chen, and P. G. Bruce, *Science*, **337**, 563 (2012).
3. R. Subbaraman, D. Strmcnik, V. Stamenkovic, and N. M. Markovic, *J. Phys. Chem. C*, **114**, 8414 (2010).
4. D. Aurbach, K. Gamolsky, B. Markovsky, Y. Gofer, M. Schmidt, and U. Heider, *Electrochimica Acta*, **47**, 1423 (2002).
5. C. Merlet, B. Rotenberg, P. A. Madden, P.-L. Taberna, P. Simon, Y. Gogotsi, and M. Salanne, *Nat. Mater.*, **11**, 306 (2012).
6. A. Balducci, R. Dugas, P. L. Taberna, P. Simon, D. Plée, M. Mastragostino, and S. Passerini, *J. Power Sources*, **165**, 922 (2007).
7. K. Mizushima, P. C. Jones, P. J. Wiseman, and J. B. Goodenough, *Mater. Res. Bull.*, **15**, 783 (1980).
8. M. L. Perry and T. F. Fuller, *J.-Electrochem. Soc.*, **149**, S59 (2002).
9. M. Ciureanu, S. Mikhailenko, and S. Kaliaguine, *Catal. Today*, **82**, 195 (2003).
10. K. Adjemian, S. Lee, S. Srinivasan, J. Benziger, and A. Bocarsly, *J. Electrochem. Soc.*, **149**, A256 (2002).
11. J. Marcicki, A. T. Conlisk, and G. Rizzoni, *J. Power Sources*, **251**, 157 (2014).
12. R. Jorn, R. Kumar, D. P. Abraham, and G. A. Voth, *J. Phys. Chem. C*, **117**, 3747 (2013).
13. V. S. Bryantsev and M. Blanco, *J. Phys. Chem. Lett.*, **2**, 379 (2011).
14. A. Frumkin, *Acta Physicochim URSS*, **18**, 23 (1943); A. N. Frumkin, *Z. Phys. Chem.*, **164A**, 121 (1933); A. N. Frumkin, *J. Electrochem. Soc.*, **107**, 461 (1960); Z. Nagy and P. F. Schultz, *J. Electrochem. Soc.*, **135**, 2700 (1988).
15. A. Frumkin and O. Petrii, *Electrochimica Acta*, **20**, 347 (1975).
16. P. M. Biesheuvel, A. A. Franco, and M. Z. Bazant, *J. Electrochem. Soc.*, **156**, B225 (2009).
17. A. Bonnefont, F. Argoul, and M. Z. Bazant, *J. Electroanal. Chem.*, **500**, 52 (2001).
18. E. Itskovich, A. Kornyshev, and M. Vorotyntsev, *Phys. Status Solidi A*, **39**, 229 (1977).
19. A. A. Kornyshev and M. A. Vorotyntsev, *Electrochimica Acta*, **23**, 267 (1978).
20. A. A. Kornyshev and M. A. Vorotyntsev, *Can. J. Chem.*, **59**, 2031 (1981).
21. J. Tomasi, B. Mennucci, and R. Cammi, *Chem. Rev.*, **105**, 2999 (2005).
22. A. A. Franco, P. Schott, C. Jallut, and B. Maschke, *J. Electrochem. Soc.*, **153**, A1053 (2006).
23. R. F. de Morais, P. Sautet, D. Loffreda, and A. A. Franco, *Electrochimica Acta*, **56**, 10842 (2011).
24. R. He, S. Chen, F. Yang, and B. Wu, *J. Phys. Chem. B*, **110**, 3262 (2006).
25. A. A. Franco, *RSC Advances*, **3**(32), 13027 (2013).
26. A. A. Franco and K. H. Xue, *ECS Journal of Solid State Science and Technology*, **2**(10), M3084 (2013).
27. K. Malek and A. A. Franco, *J. Phys. Chem. B*, **115**(25), 8088 (2011).
28. A. A. Franco, *Multiscale modeling of electrochemical devices for energy conversion and storage, book chapter in: Encyclopedia of Applied Electrochemistry*, edited by R. Savinell, K. I. Ota, and G. Kreysa (Springer, UK) (2013).
29. A. A. Franco, *Modeling of Direct Alcohol Fuel Cells, book chapter in: Direct Alcohol Fuel Cells Technologies: research and development*, edited by E. Gonzalez and H. Corti (Springer, USA) (2013).
30. A. A. Franco, PEMFC degradation modeling and analysis, book chapter in: Polymer electrolyte membrane and direct methanol fuel cell technology (PEMFCs and DMFCs) - Volume 1: *Fundamentals and performance*, edited by C. Hartnig and C. Roth (Woodhead, UK) (2012).
31. A. A. Franco, P. Schott, C. Jallut, and B. Maschke, *Fuel Cells*, **7**, 99 (2007).
32. C. O. Laoire, S. Mukerjee, K. Abraham, E. J. Plichta, and M. A. Hendrickson, *J. Phys. Chem. C*, **114**, 9178 (2010).
33. J. G. Kirkwood, *Chem. Rev.*, **24**, 233 (1939).
34. K. E. Newman, *Chem Soc Rev*, **23**, 31 (1994).
35. J. G. Kirkwood and F. P. Buff, *J. Chem. Phys.*, **19**, 774 (2004).
36. P. Wang and A. Anderko, *Fluid Phase Equilibria*, **186**, 103 (2001).
37. E. Gongadze, U. Van Rienen, and A. Iglic, *Cell. Mol. Biol. Lett.*, **16**, 576 (2011).
38. A. I. Ioanid, R. Mircea, and T. M. Ciuceanu, *Dig. J. Nanomater. Biostructures DJNB*, **6**, 1427–1434 (2011).
39. B. E. Conway, J. Bockris, and I. A. Ammar, *Trans. Faraday Soc.*, **47**, 756 (1951).
40. A. Abrashkin, D. Andelman, and H. Orland, *Phys. Rev. Lett.*, **99**, 077801 (2007).
41. E. Gongadze and A. Iglic, *Bulg J Phys*, **39**, 012 (2012).
42. E. Gongadze and A. Iglic, *Gen Physiol Biophys*, **32**, 143 (2013).
43. A. Levy, D. Andelman, and H. Orland, *Phys. Rev. Lett.*, **108**, 227801 (2012).
44. R. D. Coalson, A. M. Walsh, A. Duncan, and N. Ben-Tal, *J. Chem. Phys.*, **102**, 4584 (1995).
45. K. Andresen, R. Das, H. Y. Park, H. Smith, L. W. Kwok, J. S. Lamb, E. J. Kirkland, D. Herschlag, K. D. Finkelstein, and L. Pollack, *Phys. Rev. Lett.*, **93**, 248103 (2004).
46. I. Borukhov, D. Andelman, and H. Orland, *Phys. Rev. Lett.*, **79**, 435 (1997).
47. I. Rouzina and V. A. Bloomfield, *J. Phys. Chem.*, **100**, 4305 (1996).
48. D. Antypov, M. C. Barbosa, and C. Holm, *Phys. Rev. E*, **71**, 061106 (2005).
49. M. S. Kilic, M. Z. Bazant, and A. Ajdari, *arXiv:physics/0611232* (2006) http://arxiv.org/abs/physics/0611232.
50. M. S. Kilic, M. Z. Bazant, and A. Ajdari, *Phys. Rev. E*, **75**, 021502 (2007).
51. V. B. Chu, Y. Bai, J. Lipfert, D. Herschlag, and S. Doniach, *Biophys. J.*, **93**, 3202 (2007).
52. B. Lu and Y. C. Zhou, *Biophys. J.*, **100**, 2475 (2011).
53. J. R. Reitz, F. J. Milford, and R. W. Christy, *Foundations of electromagnetic theory*, Pearson/Addison-Wesley, San Francisco, Calif., (2009).
54. I. Borukhov, D. Andelman, and H. Orland, *Phys. Rev. Lett.*, **79**, 435 (1997).
55. F. Wang, R. Robert, N. A. Chernova, N. Pereira, F. Omenya, F. Badway, X. Hua, M. Ruotolo, R. Zhang, L. Wu, V. Volkov, D. Su, B. Key, M. S. Whittingham, C. P. Grey, G. G. Amatucci, Y. Zhu, and J. Graetz, *J. Am. Chem. Soc.*, **133**, 18828 (2011).
56. H. Wang, A. Thiele, and L. Pilon, *J. Phys. Chem. C*, **117**, 18286 (2013).
57. M. S. Kilic, M. Z. Bazant, and A. Ajdari, *Phys. Rev. E*, **75**, 021503 (2007).
58. K. T. Chu and M. Z. Bazant, *J. Colloid Interface Sci.*, **315**, 319 (2007).
59. C. Chiappe, M. Malvaldi, and C. S. Pomelli, *Pure Appl. Chem.*, **81**, 767 (2009).
60. P. Berg and B. E. Benjaminsen, *Electrochimica Acta*, **120**, 429 (2014).
61. E. Gongadze, U. van Rienen, V. Kralj-Iglic, and A. Iglic, *Gen. Physiol. Biophys.*, **30**, 130 (2011).
62. L. F. L. Oliveira, C. Jallut, and A. A. Franco, *Electrochimica Acta*, **110**, 363 (2013).
63. B. J. Kirby and E. F. Hasselbrink, *ELECTROPHORESIS*, **25**, 187 (2004).
64. K.-H. Xue, T.-K. Nguyen, and A. A. Franco, *J. Electrochem. Soc.*, **161**, E3028 (2014).
65. K. Xu, *Chem. Rev.*, **104**, 4303 (2004).
66. M. Quiroga and A. A. Franco, in preparation (2014).
67. A. A. Franco and K. Malek, in preparation (2014).